Electronic Research Archive

http://www.aimspress.com/journal/era

ERA, 31(3): 1323–1343.
DOI: 10.3934/era.2023068
Received: 22 October 2022
Revised: 12 December 2022
Accepted: 26 December 2022
Published: 09 January 2023

Research article

An adaptive finite element method based on Superconvergent Cluster Recovery for the Cahn-Hilliard equation

Wenyan Tian[1], Yaoyao Chen[2], Zhaoxia Meng[3] and Hongen Jia[1,*]

[1] College of Mathematics, Taiyuan University of Technology, Tai'yuan 030024, China

[2] School of Mathematics and Statistics, Anhui Normal University, Wu'hu 241000, China

[3] Department of energy and power engineering, Shanxi Institute of Energy, Tai'yuan 030024, China

* **Correspondence:** Email: jiahongen@aliyun.com.

Abstract: In this study, we construct an error estimate for a fully discrete finite element scheme that satisfies the criteria of unconditional energy stability, as suggested in [1]. Our theoretical findings, in more detail, demonstrate that this system has second-order accuracy in both space and time. Additionally, we offer a powerful space and time adaptable approach for solving the Cahn-Hilliard problem numerically based on the posterior error estimation. The major goal of this technique is to successfully lower the calculated cost by controlling the mesh size using a Superconvergent Cluster Recovery (SCR) approach in accordance with the error estimation. To demonstrate the effectiveness and stability of the suggested SCR-based algorithm, numerical results are provided.

Keywords: error estimate; the Cahn-Hilliard equation ; adaptive; SCR

1. Introduction

The Cahn-Hilliard equation is solved in this study using the adaptive finite element approach.

$$\begin{cases} \mathbf{u}_t = -\varepsilon\Delta^2\mathbf{u} + \dfrac{1}{\varepsilon}\Delta f(u) & \text{in } \Omega\times(0,T], \\ \partial_n\mathbf{u} = \partial_n(-\varepsilon\Delta\mathbf{u} + \dfrac{1}{\varepsilon}f(u)) = 0, & \text{on } \partial\Omega\times(0,T], \\ \mathbf{u}(x,0) = \mathbf{u}_0 & \text{in } \Omega. \end{cases} \tag{1.1}$$

In the equation above, we use to Ω signify a limited domain in $R^d(d = 2 \text{ or } 3)$ with Lipschitz boundary $\partial\Omega$, and $\mathbf{n}$ stands for the unit outward normal to $\mathbf{\Omega}$, $\mathbf{u}$ also stands for the phase-field variable that will be solved. $f(u)$ is a nonlinear function. ε is a constant. T is the ultimate time.

The Cahn-Hilliard (CH) equation, often known as the common phase field model, was first published in 1958 in a key paper by Cahn and Hillard's [2], which examined the thermodynamic phenomenon of mutual diffusion of two substances (such as alloys and polymers). In general, this equation can be used to express the intricate phase separation and coarsening phenomena in solids, especially in materials science and fluid dynamics, for examples, see [3–6] and the references therein. The Cahn-Hilliard equation, which holds multiple time scales and spatial scales, is a rigid and nonlinear fourth-order PDE. So it is challenging to identify the precise solution.

The majority of studies in recent years have focused on finite difference techniques or the Fourier-spectral approach (periodic boundary), and many authors have devoted their time to examining different Cahn-Hilliard equation versions, including the viscous Cahn-Hilliard equation, the surface Cahn-Hilliard equation, the CHNS equation, etc. and research issues from space and time that are related. Barrett and Elliott presented to study the Cahn-Hilliard system by using conforming and nonconforming finite element methods [7–9]. Shen and Xu described in [10] the treatment of the Cahn-Hilliard equation by the scalar auxiliary variable (SAV) method. Zhao and Xiao combined the surface finite element method (SFEM) with stabilized semi-implicit model to solve the surface Cahn-Hilliard model [11]. There are many parallels between the Allen-Cahn equation and the Cahn-Hilliard equation since they are phase field flows of the same energy in different regions, such as energy decreasing. In [12], Shen and Yang analyzed the discrete versions of the Allen-Cahn and Cahn-Hilliard equations. Numerous research has been conducted on the Allen-Cahn equation [13–15], and Chen and Huang applied the Superconvergent Cluster Recovery (SCR) approach for the Allen-Cahn equation [16]. The method was also used in [17] to solve the CHNS equation, but the Cahn-Hilliard equation has not yet seen this treatment. In [17], the Cahn-Hilliard component is treated as a first-order format combing with a time-space adaptive method. In our paper, we analyze the Cahn-Hilliard equation using a second-order time discrete method and convex splitting for the nonlinear factor f, combined with the SCR method.

There are two reasons why we use adaptive methods in this study. First, due to the presence of the tiny parameter ε, it produces the phenomenon of the interfacial layer. When meshing on this interfacial layer, different from other parts, we need fine encryption, and the adaptive strategy can effectively solve this problem. Second, it takes a very long time for the numerical simulation of the Cahn-Hilliard model to reach the steady state, therefore using adaptive mesh creation makes sense in terms of time and money savings. At present, numerous writers have examined the Cahn-Hilliard equation's adaptive technique, including [11], where the discrete chemical potential is employed as an error estimator to evaluate the fluctuation in numerical energy. Based on the a posteriori error estimations, the standard mesh refinement procedures were used in [18] for automatic mesh refining. In [17], the SCR based posteriori error estimators were constructed for space discretization of phase field variable and velocity function. The adaptive time-stepping method was applied to change the time step in [19, 20].

In this work, we first provide an error estimate for the second-order fully discrete technique suggested in [1]. The fully discrete scheme is then introduced with an effective time-space adaptive technique called SCR. We need understand that the SCR approach has the same or higher accuracy while being more effective and affordable than other adaptive techniques. The SCR strategy was originally proposed by Huang and Yi [21], and they applied it to the Allen-Cahn system [16]. Moreover, for the definition of error estimator, the time discretization error estimator is given by the difference of numerical approximation between adjacent time steps, and the spatial discretization

error estimator is defined by gradient, that is, the difference between the reconstructed gradient and the numerical gradient.

The remainder of the essay is structured as follows. For the Cahn-Hilliard equation, we offer a second-order fully discrete scheme in Section 2, after which we examine the error estimation and unconditional energy stability. In Section 3, we introduce the characteristics of the superconvergent cluster recovery operator, and define the error estimation operator in time and space. Several numerical tests illustrate the effectiveness of our adaptive procedure in Section 4.

2. This energy-stabilized discrete model

First of all, we introduce a new variable $\mu =: -\varepsilon\Delta\mathbf{u} + \frac{1}{\varepsilon}f(u)$ and rewrite Eq (1.1) as follows.

$$\begin{cases} \mathbf{u}_t = \Delta\mu & \text{in } \Omega \times (0, T], \\ \mu = -\varepsilon\Delta\mathbf{u} + \dfrac{1}{\varepsilon}f(u) & \text{in } \Omega \times (0, T], \\ \partial_n\mathbf{u} = \partial_n\mu = 0 & \text{on } \partial\Omega \times (0, T], \\ \mathbf{u}(x, 0) = \mathbf{u}_0 & \text{in } \Omega, \end{cases} \tag{2.1}$$

where $\varepsilon > 0$ is a small parameter, which represents the thickness of the transition interface between materials, and $\mathbf{u}$ means the phase field variable, $\mathbf{u_0} \in H^1(\Omega)$ as the initial value at $t = 0$. The solution is driven into the two pure states $u = \pm 1$ by the nonlinear part $f(u) = F'(u)$, and $F(u)$ is a double-well potential function, which is given by $F(u) = \frac{1}{4}(u^2 - 1)^2$.

Actually, the Cahn-Hilliard equation could be viewed as the $H^{-1}-$gradient flow of the free energy $E(u)$:

$$E(u) = \int_\Omega (\frac{1}{\varepsilon}F(u) + \frac{\varepsilon}{2}|\nabla u|^2)dx, \tag{2.2}$$

Furthermore, by a simple mathematical derivation, for the Cahn-Hilliard equation, the following energy law can be derived:

$$\frac{d}{dt}E(u) = -\int_\Omega |\nabla(-\varepsilon\Delta u + \frac{1}{\varepsilon}f(u))|^2 dx \le 0, \tag{2.3}$$

that the energy-decreasing property is satisfied by the free energy $E(u)$, over time,

$$E(u)(t^{n+1}) \le E(u)(t^n), \quad \forall\, n \in \mathbb{N}. \tag{2.4}$$

Besides, the Cahn-Hilliard equation satisfies the law of conservation of mass [2].

$$\frac{d}{dt}\int_\Omega u(x, t)dx = 0, \quad 0 \le t \le \mathrm{T}. \tag{2.5}$$

Next, we will present a few notations that will be used all across the paper before we get started. The standard Sobolev space will be indicated by the notation $H^m = W^{m,2}(\Omega)$, and its associated norm of H^m can be represented by $\|\cdot\|_m$. As well as $\|\cdot\|$ and $(\cdot, \cdot)$ respectively stand in for norm and the inner product of L^2. Besides, we use the symbol $\|\cdot\|_\infty$ to signify the L^∞ norm.

Let size h be the largest element diameter for every e_h and $\mathcal{T}_h = \{e_h\}$ be the set of regularly shaped triangles. Let V_h be the corresponding space in finite dimensions for piecewise linear continuous functions:

$$V_h = \{v \in H^1(\Omega) : v|_{e_h} \in P_1(e_h),\ \forall e_h \in \mathcal{T}_h\},$$

and its basis functions are the standard Lagrange basis functions $\phi_z(z \in \mathcal{N}_h$, where the $\mathcal{N}_h$ represents the set of the triangular vertices). Naturally, we denote $V_h^0 = V_h \bigcap H_0^1(\Omega)$.

In addition, for the real number $p \geq 0$ and satisfying the condition $v(t)$, we define the following norm:

$$\|v\|_{L_p(0,T;X)} = (\int_0^T \|v(t)\|_X^p dt)^{\frac{1}{2}}.$$

Then, by using the above symbol, we first introduce the weak form of Eq (2.1), which is as follow: find $\mathbf{u} \in L^\infty(0,T;H^1(\Omega))$, $w \in L^2(0,T;H^1(\Omega))$

$$\begin{cases} (\mathbf{u}_t, w) + (\nabla\mu, \nabla w) = 0 & \forall\ w\ \in\ H^1(\Omega), \\ (\mu\ , v) = \varepsilon(\nabla\mathbf{u}, \nabla v) + \dfrac{1}{\varepsilon}(f(u), v) & \forall\ v\ \in\ H^1(\Omega), \\ (\mathbf{u}(0) - \mathbf{u}_0, q) = 0 & \forall\ q\ \in\ H^1(\Omega). \end{cases} \tag{2.6}$$

To solve Eq (2.6), the semi-discrete system needs to find $\mathbf{u}_h \in C^1(0,T;V_h)$

$$\begin{cases} (\mathbf{u}_{h,t}, w_h) + (\nabla\mu_h, \nabla w_h) = 0 & \forall\ w_h\ \in\ V_h, \\ (\mu_h\ , v_h) = \varepsilon(\nabla\mathbf{u_h}, \nabla v_h) + \dfrac{1}{\varepsilon}(f(u_h), v_h) & \forall\ v_h\ \in\ V_h, \\ (\mathbf{u_h}(0) - \mathbf{u_{h0}^0}, q_h) = 0 & \forall\ q_h\ \in\ V_h, \end{cases} \tag{2.7}$$

where $\mathbf{u}_h^0$ is an approximation of $\mathbf{u}_0$ in V_h.

Divide $[0,T]$ into N_{st} subintervals $I_n := (t^{n-1}, t^n]$, uniformly, $0 = t^0 < t^1 < ... < t^N = T$. Let $\triangle t$ represent the time step size so $T = N\triangle t$, $n = 1, ..., N$. The fully discrete scheme for the nonlinear approximation, which is developed from a modified Crank-Nicolson approach, is as follows: find $u_h^n \in V_h^n, n = 1, 2, ..., N$

$$\begin{cases} (\dfrac{\mathbf{u}_h^n - \Pi_n\mathbf{u}_h^{n-1}}{\triangle t}, w_h) + (\nabla\mu_h^{n-\frac{1}{2}}, \nabla w_h) = 0 & \forall\ w_h\ \in\ V_h^n, \\ (\mu_h^{n-\frac{1}{2}}\ , v_h) = \varepsilon(\nabla\widehat{\mathbf{u}_\mathbf{h}^\mathbf{n}}, \nabla v_h) + \dfrac{1}{\varepsilon}(f(u_h^n, u_h^{n-1}), v_h) & \forall\ v_h\ \in\ V_h^n, \\ (\mathbf{u}_h(0) - \mathbf{u_{h0}^0}, q_h) = 0 & \forall\ q_h\ \in\ V_h^0, \end{cases} \tag{2.8}$$

where $\widehat{u_h^n}$, and $f(u_h^n, u_h^{n-1})$ are defined as

$$\begin{aligned} \widehat{u_h^n} &= \frac{u_h^n + \Pi_n u_h^{n-1}}{2}, \\ f(u_h^n, u_h^{n-1}) &= \frac{(u_h^n)^3 + (u_h^n)^2\Pi_n u_h^{n-1} + u_h^n(\Pi_n u_h^{n-1})^2 + (\Pi_n u_h^{n-1})^3}{4} - \frac{u_h^n + \Pi_n u_h^{n-1}}{2}, \end{aligned} \tag{2.9}$$

as well as $\mu^{n-\frac{1}{2}}$ is the approximation at the midpoint $t^{n-\frac{1}{2}} = (t^{n-1} + t^n)/2$ (directly computed), and Π_n represents the interpolation into the finite element space V_h. Next, we consider the mass conservative, taking $w_h = 1$ in (2.8), the following results can be easily obtained

$$\int_\Omega u^n = \int_\Omega u^{n-1} = \int_\Omega u^0.$$

Obviously, the fully discrete scheme is mass conservative.

In addition, We use the convex partitioning method to divide f into two parts, i.e., the linear convex part and the nonlinear concave part. The linear convex part is then handled by the modified Crank-Nicolson method, while the linear convex part is handled by the Midpoint approximation (MP) method. So far, the modified Crank-Nicolson method has been applied several times to the Cahn-Hilliard equation to deal with the nonlinear concave terms, such as [22–25], and the linear convex terms in these works of literature are treated by BDF2.

Lemma 2.1. *(Discrete Gronwall lemma) [26]. Let C and $\triangle t$ be non-negative constants, and a_k, b_k, c_k, d_k be non-negative sequences satisfying*

$$a_k + \triangle t \sum_{k=0}^{n} b_k \le \triangle t \sum_{k=0}^{n-1} d_k a_k + \triangle t \sum_{k=0}^{n-1} c_k + C_0, \ \forall n \ge 1,$$

then

$$a_n + \triangle t \sum_{k=0}^{n} b_k \le exp(\triangle t \sum_{k=0}^{n-1} d_k)(\triangle t \sum_{k=0}^{n-1} c_k + C_0), \ \forall n \ge 1.$$

Theorem 2.1. *The solution of the fully discrete scheme Eqs (2.8) and (2.9), which is unconditionally energy stable, satisfies*

$$E(u_h^n) \le E(u_h^{n-1}), \ \ \forall n \ge 1.$$

Proof. Taking $w_h = \triangle t \mu_h^{n-\frac{1}{2}}$ and $v_h = u_h^n - u_h^{n-1}$ in Eq (2.8) we obtain

$$\begin{cases} (u_h^n - u_h^{n-1}, \mu_h^{n-\frac{1}{2}}) + \triangle t \|\nabla \mu_h^{n-\frac{1}{2}}\|^2 = 0, \\ (\mu_h^{n-\frac{1}{2}}, u_h^n - u_h^{n-1}) = \dfrac{\varepsilon}{2}(\|\nabla u_h^n\|^2 - \|\nabla u_h^{n-1}\|^2) + \dfrac{1}{\varepsilon}(f(u_h^n, u_h^{n-1}), u_h^n - u_h^{n-1}), \end{cases}$$

where

$$\begin{aligned} \frac{1}{\varepsilon}(f(u_h^n, u_h^{n-1}), u_h^n - u_h^{n-1}) &= \frac{1}{\varepsilon}(\frac{(u_h^n)^3 + (u_h^n)^2 u_h^{n-1} + u_h^n (u_h^{n-1})^2 + (u_h^{n-1})^3}{4} - \frac{u_h^n + u_h^{n-1}}{2}, u_h^n - u_h^{n-1}) \\ &= \frac{1}{\varepsilon} \int \frac{1}{4}(u_h^n)^4 - \frac{1}{4}(u_h^{n-1})^4 - \frac{1}{2}(u_h^n)^2 + \frac{1}{2}(u_h^{n-1})^2 dx, \end{aligned}$$

by integrating the upper formula, we obtain

$$0 = \triangle t\|\nabla\mu_h^{n-\frac{1}{2}}\|^2 + \frac{\varepsilon}{2}(\|\nabla u_h^n\|^2 - \|\nabla u_h^{n-1}\|^2) + \frac{1}{\varepsilon}\int \frac{1}{4}(u_h^n)^4 - \frac{1}{4}(u_h^{n-1})^4 - \frac{1}{2}(u_h^n)^2 + \frac{1}{2}(u_h^{n-1})^2 dx.$$

Also for energy we have

$$\begin{aligned} E(u_h^n) - E(u_h^{n-1}) &= \int \frac{1}{\varepsilon}F(u_h^n) + \frac{\varepsilon}{2}|\nabla u_h^n|^2 - \frac{1}{\varepsilon}F(u_h^{n-1}) + \frac{\varepsilon}{2}|\nabla u_h^{n-1}|^2 dx \\ &= \frac{1}{\varepsilon}\int \frac{1}{4}(u_h^n)^4 - \frac{1}{4}(u_h^{n-1})^4 - \frac{1}{2}(u_h^n)^2 + \frac{1}{2}(u_h^{n-1})^2 dx + \frac{\varepsilon}{2}(\|\nabla u_h^n\|^2 - \|u_h^{n-1}\|^2), \end{aligned}$$

the equation is finally obtained

$$\triangle t\|\nabla\mu_h^{n-\frac{1}{2}}\|^2 + E(u_h^n) - E(u_h^{n-1}) = 0,$$

which means that the energy-decreasing feature is maintained by the provided fully discrete scheme Eqs (2.8) and (2.9). We omit Π_n since it implies interpolation into the finite element space V_h^n and has no bearing on the theoretical derivation procedure.

To derive the error estimates, we define the elliptic projection operator as $P_h : H^1 \to V_h$, which satisfies

$$(\nabla(P_h v - v), \nabla\alpha_h) = 0, \quad \forall\alpha_h \in V_h. \tag{2.10}$$

From the literature [27], we know the following two inequalities hold,

$$\|v - P_h v\| \le Ch^2\|v\|_2, \quad \|(v - P_h v)_t\| \le Ch^2\|v_t\|_2. \tag{2.11}$$

Then, we denote the error functions as,

$$\begin{aligned} &\tilde{e}^n = P_h u(t^n) - u_h^n, \quad \hat{e}^n = u(t^n) - P_h u(t^n), \\ &\bar{e}^{n-\frac{1}{2}} = P_h\mu(t^{n-\frac{1}{2}}) - \mu_h^{n-\frac{1}{2}}, \quad \breve{e}^{n-\frac{1}{2}} = \mu(t^{n-\frac{1}{2}}) - P_h\mu(t^{n-\frac{1}{2}}). \end{aligned}$$

We may quickly derive by using the Taylor expansion with integral residuals and Young's inequality [12].

$$\|R_1^n\|_s^2 \le \triangle t^3 \int_{t^{n-1}}^{t^n} \|u_{ttt}(t)\|_s^2 dt, \, s = -1, 0, \tag{2.12}$$

$$\|R_2^n\|_s^2 \le \triangle t^3 \int_{t^{n-1}}^{t^n} \|u_{tt}(t)\|_{s+2}^2 dt, \, s = -1, 0, \tag{2.13}$$

where

$$R_1^n = \frac{u(t^n) - u(t^{n-1})}{\triangle t} - u_t(t^{n-\frac{1}{2}}),$$

$$R_2^n = -\triangle(\frac{u(t^n) + u(t^{n-1})}{2} - u(t^{n-\frac{1}{2}})).$$

Theorem 2.2. *Let u_h^n and $u(t^n)$ represent, respectively, the solutions of Eqs (2.8), (2.9) and (2.1). After that, for $u \in C(0,T;H^2(\Omega))$, $u_t \in L^2(0,T;H^2(\Omega)) \bigcap L^2(0,T;L^4(\Omega))$, $u_{tt} \in L^2(0,T;H^1(\Omega))$, and $u_{ttt} \in L^2(0,T;H^{-1}(\Omega))$ we get*

$$\|u_h^k - u(t^k)\| + (\frac{\triangle t}{\varepsilon}\sum_{n=0}^{k}\|\mu_h^{n-\frac{1}{2}} - \mu(t^{n-\frac{1}{2}})\|^2)^{\frac{1}{2}} \leqslant C(\varepsilon,T)(K_1(\varepsilon,u)\triangle t^2 + K_2(\varepsilon,u)h^2),$$

where

$$\begin{aligned}
&C(\varepsilon,T) \sim exp(T\backslash\varepsilon),\\
&K_1(\varepsilon,u) = \sqrt{\varepsilon}(\|u_{ttt}\|_{L^2(0,T;H^{-1})} + \|u_{tt}\|_{L^2(0,T;H^1)})\\
&\qquad\qquad + \frac{1}{\sqrt{\varepsilon}}(\|u_{tt}\|_{L^2(0,T;L^2)} + \|u_t\|_{L^2(0,T;L^4)}),\\
&K_2(\varepsilon,u) = \|u_0\|_2 + \sqrt{\varepsilon}\|u_t\|_{L^2(0,T;H^2)} + \frac{1}{\sqrt{\varepsilon}}\|\mu\|_{C(0,T;H^2)} + \|u\|_{C(0,T;H^2)}.
\end{aligned}$$

Proof. Subtracting Eq (2.8) from the weak form of Eq (2.6) on Ω at $t^{n-\frac{1}{2}}$, we obtain

$$\begin{aligned}
&\frac{1}{\triangle t}(\tilde{e}^n - \tilde{e}^{n-1}, w_h) + (\nabla\bar{e}^{n-\frac{1}{2}}, \nabla w_h) = (R_1^n - \frac{1}{\triangle t}(I - P_h)(u(t^n) - u(t^{n-1})), w_h),\\
&(\bar{e}^{n-\frac{1}{2}} + \check{e}^{n-\frac{1}{2}}, v_h) = \frac{\varepsilon}{2}(\nabla\tilde{e}^n + \nabla\tilde{e}^{n-1}, v_h) + \varepsilon(\triangle R_2^n, v_h) + \frac{1}{\varepsilon}(f(u(t^{n-\frac{1}{2}})) - f(u_h^n, u_h^{n-1}), v_h),
\end{aligned}$$

then taking $w_h = \frac{1}{2}\varepsilon\triangle t(\tilde{e}^n + \tilde{e}^{n-1})$ and $v_h = \triangle t\bar{e}^{n-\frac{1}{2}}$ respectively, and summing up the two identities above, we gain

$$\begin{aligned}
&\|\tilde{e}^n\|^2 - \|\tilde{e}^{n-1}\|^2 + \frac{2\triangle t}{\varepsilon}\|\bar{e}^{n-\frac{1}{2}}\|^2\\
&= \triangle t(R_1^n, \tilde{e}^n + \tilde{e}^{n-1}) - (I - P_h)(u(t^n) - u(t^{n-1}), \tilde{e}^n + \tilde{e}^{n-1}) - 2\triangle t(R_2^n, \bar{e}^{n-\frac{1}{2}})\\
&\quad + \frac{2\triangle t}{\varepsilon^2}(f(u(t^{n-\frac{1}{2}})) - f(u_h^n, u_{n-1}^n), \bar{e}^{n-\frac{1}{2}}) - \frac{2\triangle t}{\varepsilon}(\check{e}^{n-\frac{1}{2}}, \bar{e}^{n-\frac{1}{2}})\\
&:= \mathbf{I} + \mathbf{II} + \mathbf{III} + \mathbf{IV} + \mathbf{V},
\end{aligned}$$

where

$$\begin{aligned}
&\mathbf{I} := \triangle t(R_1^n, \tilde{e}^n + \tilde{e}^{n-1}),\\
&\mathbf{II} := -(I - P_h)(u(t^n) - u(t^{n-1}), \tilde{e}^n + \tilde{e}^{n-1}),\\
&\mathbf{III} := -2\triangle t(R_2^n, \bar{e}^{n-\frac{1}{2}}),\\
&\mathbf{IV} := \frac{2\triangle t}{\varepsilon^2}(f(u(t^{n-\frac{1}{2}})) - f(u_h^n, u_h^{n-1}), \bar{e}^{n-\frac{1}{2}}),\\
&\mathbf{V} := -\frac{2\triangle t}{\varepsilon}(\check{e}^{n-\frac{1}{2}}, \bar{e}^{n-\frac{1}{2}}).
\end{aligned}$$

the Cauchy inequality with ε and Young's inequality were used to estimate **I**, **II**, **III**, and **V** as following:

$$
\begin{aligned}
\mathbf{I} &\le \triangle t\|R_1^n\|\|\tilde{e}^n+\tilde{e}^{n-1}\| \le \frac{\triangle t}{2}(\varepsilon\|R_1^n\|^2+\frac{1}{\varepsilon}\|\tilde{e}^n+\tilde{e}^{n-1}\|^2)\\
&\le \frac{\varepsilon\triangle t^4}{2}\int_{t^{n-1}}^{t^n}\|u_{ttt}(t)\|_{-1}^2dt+\frac{\triangle t}{2\varepsilon}\|\tilde{e}^n\|^2+\frac{\triangle t}{2\varepsilon}\|\tilde{e}^{n-1}\|^2,\\
\mathbf{II} &\le \|(I-P_h)(u(t^n)-u(t^{n-1}))\|\|\tilde{e}^n+\tilde{e}^{n-1}\|\\
&\le \frac{\varepsilon}{2}\int_{t^{n-1}}^{t^n}\|(I-P_h)u_t(t)\|^2dt+\frac{1}{2\varepsilon}\|\tilde{e}^n\|^2+\frac{1}{2\varepsilon}\|\tilde{e}^{n-1}\|^2,\\
\mathbf{III} &\le 3\triangle t\varepsilon\|R_2^n\|^2+\frac{\triangle t}{3\varepsilon}\|\bar{e}^{n-\frac{1}{2}}\|^2 \le 3\varepsilon\triangle t^4\int_{t^{n-1}}^{t^n}\|u_{tt}(t)\|_1^2dt+\frac{\triangle t}{3\varepsilon}\|\bar{e}^{n-\frac{1}{2}}\|^2,\\
\mathbf{V} &\le \frac{2\triangle t}{\varepsilon}(\sqrt{3}\|\check{e}^{n-\frac{1}{2}}\|)(\frac{1}{\sqrt{3}}\|\bar{e}^{n-\frac{1}{2}}\|) \le \frac{3\triangle t}{\varepsilon}\|\check{e}^{n-\frac{1}{2}}\|^2+\frac{\triangle t}{3\varepsilon}\|\bar{e}^{n-\frac{1}{2}}\|^2.
\end{aligned}
$$

For simplicity, we denote $u(t^n)=u_n$ and $u(t^{n-\frac{1}{2}})=u_{n-\frac{1}{2}}$. We consider the fourth term IV as follows:

$$
\begin{aligned}
\mathbf{IV} &= \frac{2\triangle t}{\varepsilon^2}(f(u_{n-\frac{1}{2}})-f(u_h^n-u_h^{n-1}),\bar{e}^{n-\frac{1}{2}})\\
&= \frac{2\triangle t}{\varepsilon^2}(\frac{u_h^n-u_h^{n-1}}{2}-u_{n-\frac{1}{2}}+(u_{n-\frac{1}{2}})^3-\frac{(u_h^n)^3+(u_h^n)^2u_h^{n-1_h}+u_h^n(u_h^{n-1})^2+(u_h^{n-1})^3}{4})\\
&= \frac{2\triangle t}{\varepsilon^2}(\frac{u_h^n-u_h^{n-1}}{2}-u_{n-\frac{1}{2}}+(u_{n-\frac{1}{2}})^3-(\frac{u_n-u_{n-1}}{2})^3+(\frac{u_n-u_{n-1}}{2})^3-g^n\\
&\quad +g^n-\frac{(u_h^n)^3+(u_h^n)^2u_h^{n-1}+u_h^n(u_h^{n-1})^2+(u_h^{n-1})^3}{4},\bar{e}^{n-\frac{1}{2}})\\
&:= \frac{2\triangle t}{\varepsilon^2}(\mathbf{IV}_1+\mathbf{IV}_2+\mathbf{IV}_3+\mathbf{IV}_4,\bar{e}^{n-\frac{1}{2}}),
\end{aligned}
$$

where

$$
\begin{aligned}
g^n &= \frac{(u_n)^3+(u_n)^2u_{n-1}+u_n(u_{n-1})^2+(u_{n-1})^3}{4},\\
\mathbf{IV_1} &:= \frac{u_h^n+u_h^{n-1}}{2},\quad \mathbf{IV_2} := (u_{n-\frac{1}{2}})^3-(\frac{u_n+u_{n-1}}{2})^3,\\
\mathbf{IV_3} &:= (\frac{u_n+u_{n-1}}{2})^3-g^n,\quad \mathbf{IV_4} := g^n-\frac{(u_h^n)^3+(u_h^n)^2u_h^{n-1}+u_h^n(u_h^{n-1})^2+(u_h^{n-1})^3}{4}.
\end{aligned}
$$

We continue our analysis of these four terms using the Taylor expansion with integral remainders, Cauchy-Schwarz inequality, and Eqs (2.12) and (2.13), we arrive at:

$$
\begin{aligned}
\|\mathbf{IV_1}\| &= \|\frac{-\tilde{e}^n-\hat{e}^n-\tilde{e}^{n-1}-\hat{e}^{n-1}+u_n+u_{n-1}}{2}-u_{n-\frac{1}{2}}\|\\
&\le \|\frac{\tilde{e}^n+\tilde{e}^{n-1}}{2}\|+\|\frac{\hat{e}^n+\hat{e}^{n-1}}{2}\|+\|\frac{u_n+u_{n-1}}{2}-u_{n-\frac{1}{2}}\|\\
&\le \|\frac{\tilde{e}^n+\tilde{e}^{n-1}}{2}\|+\|\frac{\hat{e}^n+\hat{e}^{n-1}}{2}\|+\triangle t^3\int_{t^{n-1}}^{t^n}\|u_{tt}(t)\|^2dt,
\end{aligned}
$$

$$\begin{aligned}\|\mathbf{IV_2}\| &= \|(u_{n-\frac{1}{2}})^3 - (\frac{u_n + u_{n-1}}{2})^3\| \\ &\leq \|3\xi_1^2(\frac{u_n + u_{n-1}}{2} - u_{n-\frac{1}{2}})\| \\ &\leq 3\xi_1^2 \triangle t^3 \int_{t^{n-1}}^{t^n} \|u_{tt}(t)\|^2 dt,\end{aligned}$$

$$\begin{aligned}\|\mathbf{IV_3}\| &= \|\frac{(u_n)^3 - (u_n)^2 u_{n-1} - u_n(u_{n-1})^2 + (u_{n-1})^3}{8}\| \\ &= \|\frac{((u_n)^2 - (u_{n-1})^2)(u_n - u_{n-1})}{8}\| \\ &\leq \|\frac{\xi_2}{4}(u_n - u_{n-1})^2\| \\ &\leq \frac{\xi_2}{4}\triangle t^3 \int_{t^{n-1}}^{t^n} \|u_t^2(t)\|^2 dt,\end{aligned}$$

where ξ_1 lies between $(u_n + u_{n-1})/2$ and $u_{n-\frac{1}{2}}$, ξ_2 lies between u_n and u_{n-1}, ζ_1 and ζ_2 are located between u_{n-1} and u_n.

$$\begin{aligned}\|\mathbf{IV_4}\| &= \frac{1}{4}\|\frac{2}{3}(u_n)^3 + \frac{1}{3}(u_n + u_{n-1})^3 + \frac{2}{3}(u_{n-1})^3 - \frac{2}{3}(u_h^n)^3 + \frac{1}{3}(u_h^n + u_h^{n-1})^3 + \frac{2}{3}(u_h^{n-1})^3\| \\ &= \|\frac{1}{6}((u_n)^3 - (u_h^n)^3) + \frac{1}{6}((u_{n-1})^3 - (u_h^{n-1})^3) + \frac{1}{12}((u_n + u_{n-1})^3 - (u_h^n + u_h^{n-1})^3)\| \\ &\leq \frac{1}{2}\|\xi_3^2(u_n - u_h^n)\| + \frac{1}{2}\|\xi_4^2(u_{n-1} - u_h^{n-1})\| + \frac{1}{4}\|\xi_5^2(u_n - u_h^n + u_{n-1} - u_h^{n-1})\| \\ &\leq C(\|u_{n-1} - u_h^{n-1}\| + \|u_n - u_h^n\|) \\ &\leq C(\|\hat{e}^{n-1} + \tilde{e}^{n-1}\| + \|\hat{e}^n + \tilde{e}^n\|) \\ &\leq C(\|\hat{e}^{n-1}\| + \|\tilde{e}^{n-1}\| + \|\hat{e}^n\| + \|\tilde{e}^n\|),\end{aligned}$$

where ξ_3 lies between u_n and u_{n-1}, ξ_4 lies between u_{n-1} and u_h^{n-1}, and ξ_5 lies between $u_n + u_{n-1}$ and $u_h^n + u_h^{n-1}$. To guarantee the existence of ξ_3, ξ_4, ξ_5, we need the condition [28] (Suppose C, a positive constant that is unaffected by $\triangle t$ or h, exists).

$$\|u_h^n\|_\infty \leq C, \quad \forall 1 \leq n \leq N.$$

Further, combining the above inequalities $\mathbf{IV}_i, i = 1, 2, 3, 4$ into $\mathbf{IV}$, we arrive at

$$
\begin{aligned}
\mathbf{IV} &= \frac{2\triangle t}{\varepsilon^2}(\mathbf{IV_1}+\mathbf{IV_2}+\mathbf{IV_3}+\mathbf{IV_4},\bar{e}^{n-\frac{1}{2}})\\
&\le \frac{2\triangle t}{\varepsilon^2}\|\mathbf{IV_1}+\mathbf{IV_2}+\mathbf{IV_3}+\mathbf{IV_4}\|\|\bar{e}^{n-\frac{1}{2}}\|\\
&\le \frac{2\triangle t}{\varepsilon^2}(\|\mathbf{IV_1}\|+\|\mathbf{IV_2}\|+\|\mathbf{IV_3}\|+\|\mathbf{IV_4}\|)\|\bar{e}^{n-\frac{1}{2}}\|\\
&\le \frac{2\triangle t}{\varepsilon^2}(\|\frac{\tilde{e}^n+\tilde{e}^{n-1}}{2}\|+\|\frac{\hat{e}^n+\hat{e}^{n-1}}{2}\|+\triangle t^3\int_{t^{n-1}}^{t^n}\|u_{tt}(t)\|^2dt+3\xi_1^2\triangle t^3\int_{t^{n-1}}^{t^n}\|u_{tt}(t)\|^2dt\\
&\quad+\frac{\xi_2}{4}\triangle t^3\int_{t^{n-1}}^{t^n}\|u_t^2(t)\|^2dt+C(\|\hat{e}^{n-1}\|+\|\tilde{e}^{n-1}\|+\|\hat{e}^n\|+\|\tilde{e}^n\|))\|\bar{e}^{n-\frac{1}{2}}\|\\
&\le \frac{3\triangle t}{\varepsilon}(\|\frac{\tilde{e}^n+\tilde{e}^{n-1}}{2}\|+\|\frac{\hat{e}^n+\hat{e}^{n-1}}{2}\|+\triangle t^3\int_{t^{n-1}}^{t^n}\|u_{tt}(t)\|^2dt+3\xi_1^2\triangle t^3\int_{t^{n-1}}^{t^n}\|u_{tt}(t)\|^2dt\\
&\quad+\frac{\xi_2}{4}\triangle t^3\int_{t^{n-1}}^{t^n}\|u_t^2(t)\|^2dt+C(\|\hat{e}^{n-1}\|+\|\tilde{e}^{n-1}\|+\|\hat{e}^n\|+\|\tilde{e}^n\|))^2+\frac{\triangle t}{3\varepsilon}\|\bar{e}^{n-\frac{1}{2}}\|^2\\
&\le \frac{C\triangle t^4}{\varepsilon}\int_{t^{n-1}}^{t^n}\|u_{tt}(t)\|^2dt+\frac{C\triangle t^4}{\varepsilon}\int_{t^{n-1}}^{t^n}\|u_t^2(t)\|^2dt\\
&\quad+C(\|\hat{e}^{n-1}\|^2+\|\tilde{e}^{n-1}\|^2+\|\hat{e}^n\|^2+\|\tilde{e}^n\|^2)+\frac{\triangle t}{3\varepsilon}\|\bar{e}^{n-\frac{1}{2}}\|^2.
\end{aligned}
$$

Moreover, when we combine the terms **I**, **II**, **III**, **IV** and **V**, we arrive at the following estimates,

$$
\begin{aligned}
&\|\tilde{e}^n\|^2-\|\tilde{e}^{n-1}\|^2+\frac{2\triangle t}{\varepsilon}\|\bar{e}^{n-\frac{1}{2}}\|^2\\
&\le \frac{\varepsilon\triangle t^4}{2}\int_{t^{n-1}}^{t^n}\|u_{ttt}(t)\|_{-1}^2dt+\frac{\varepsilon}{2}\int_{t^{n-1}}^{t^n}\|(I-P_h)u_{tt}(t)\|^2dt+\frac{3\triangle t}{\varepsilon}\|\check{e}^{n-\frac{1}{2}}\|^2\\
&\quad+\frac{\triangle t}{3\varepsilon}\|\bar{e}^{n-\frac{1}{2}}\|^2+\frac{C\triangle t^4}{\varepsilon}\int_{t^{n-1}}^{t^n}\|u_{tt}(t)\|^2dt+\frac{C\triangle t^4}{\varepsilon}\int_{t^{n-1}}^{t^n}\|u_t^2(t)\|^2dt\\
&\quad+3\varepsilon\triangle t^4\int_{t^{n-1}}^{t^n}\|u_{tt}(t)\|_1^2dt+\frac{\triangle t}{3\varepsilon}\|\bar{e}^{n-\frac{1}{2}}\|^2\\
&\quad+C(\|\hat{e}^{n-1}\|^2+\|\tilde{e}^{n-1}\|^2+\|\hat{e}^n\|^2+\|\tilde{e}^n\|^2)+\frac{\triangle t}{3\varepsilon}\|\bar{e}^{n-\frac{1}{2}}\|^2.
\end{aligned}
$$

Using Eq (2.11), we may add up the aforementioned inequality for $n = 1, ..., k$ ($k \le T/\triangle t$), and we find,

$$
\begin{aligned}
&\|\tilde{e}^k\|^2 - \|\tilde{e}^0\|^2 + \frac{\triangle t}{\varepsilon}\sum_{n=1}^{k}\|\bar{e}^{n-\frac{1}{2}}\|^2 \\
&\leq \frac{1}{2}\triangle t^4\varepsilon\|u_{ttt}(t)\|^2_{L^2(0,T;H^{-1})} + \frac{\varepsilon}{2}Ch^4\|u_t(t)\|^2_{L^2(0,T;H^2)} + \frac{3\triangle t}{\varepsilon}\sum_{n=1}^{k}\|\breve{e}^{n-\frac{1}{2}}\|^2 \\
&\quad + \frac{C\triangle t^4}{\varepsilon}\|u_{tt}(t)\|^2_{L^2(0,T;L^2)} + C\frac{\triangle t^4}{\varepsilon}\|u_t(t)\|_{L^2(0,T;L^4)} + 3\varepsilon\triangle t^4\|u_{tt}(t)\|^2_{L^2(0,T;H^1)} \\
&\quad + C\sum_{n=1}^{k}(\|\hat{e}^{n-1}\|^2 + \|\tilde{e}^{n-1}\|^2 + \|\hat{e}^n\|^2 + \|\tilde{e}^n\|^2).
\end{aligned}
$$

Lastly, by using the triangular inequality and the discrete Gronwall lemma to the above inequality, we may conclude the proof.

3. A posteriori error estimation based SCR

The SCR technique takes derivatives to determine the recovered gradient at recovered locations after fitting a linear polynomial to solution values in a set of suitable sampling points around the vertex. In comparison to other methods, the SCR recovery technique implements adaptive algorithms more simply while saving on computing costs. The crucial component of the SCR technique is the introduction of a posterior error estimate operator. The process for getting the recovered gradient, which is broken down into three parts, is described in the sections that follow.

Step1 : We plan to restore the gradient of an interior vertex $a = a_0 \in \mathcal{N}_h$ in Ω ($\mathcal{N}_h$ represents the mesh nodes), try to choose some points symmetrically distributed around z, and then form a new point set $A = \{a_i = (x_i, y_i)\}$, $1 \leq i \leq n$ ($n \geq 4$). Specially, if select mesh nodes, we will get better results.

Step2 : The recovery gradient operator $G_h : V_h \to V_h \times V_h$ is defined as follows

$$(G_h u_h)(a) = \nabla p_a(x, y).$$

Let K_z represent the sample points of convex polygons, the linear polynomial $p_a(x, y)$ can be found

$$p_a(x, y) := \ arg\ min_{p_1 \in P_1}\sum_{i=0}^{n}(p_1(a_i) - u_h(a_i))^2,$$

In order to overcome the instability caused by small parameter h, we denote F by

$$F : \ (x, y) \to (\psi, \varphi) = \frac{(x, y) - (x_0, y_0)}{h},$$

where $h := max\{|x_i - x_0|, \ |y_i - y_0|\}$, $i = 1, 2, ..., n$. Then the fitting polynomial can be written as

$$p_a(x, y) = \mathbf{P}^T\mathbf{m} = \hat{\mathbf{P}}^T\hat{\mathbf{m}},$$

with

$$\mathbf{P}^T = (1, x, y), \quad \hat{\mathbf{P}}^T = (2, \psi, \varphi),$$
$$\mathbf{m}^T = (m_1, m_2, m_3), \quad \hat{\mathbf{m}}^T = (\hat{m}_1, \hat{m}_2, \hat{m}_3).$$

This $\hat{m}$ is the coefficient vector, it satisfies the linear systems

$$\mathbf{A}^T\mathbf{A}\hat{\mathbf{m}} = \mathbf{A}^T u,$$

where

$$\mathbf{A} = \begin{pmatrix} 1 & \psi_0 & \varphi_0 \\ 1 & \psi_1 & \varphi_1 \\ \vdots & \vdots & \vdots \\ 1 & \psi_n & \varphi_n \end{pmatrix} \quad and \quad u = \begin{pmatrix} u(a_0) \\ u(a_1) \\ \vdots \\ u(a_n) \end{pmatrix}.$$

Finally, the recovered gradient can be derived

$$G_h u = \nabla p_a = \begin{pmatrix} m_2 \\ m_3 \end{pmatrix} = \frac{1}{h}\begin{pmatrix} \hat{m}_2 \\ \hat{m}_3 \end{pmatrix}$$

Step3 : the recovered gradient $G_h u$ on Ω is obtained by the interpolation

$$G_h u = \sum_{a \in \mathcal{N}_h} G_h u(a)\phi_a.$$

Next, the following are the properties of the operator G_h was proved in [21].

a. For $e_h \in \mathcal{T}_h$, there is a constant C which is independent of the value of h, satisfied

$$\|G_h v\|_{0,e_h} \le C|v|_{1,K} \quad \forall v \in V_h,$$

where $K = \bigcup_{i=1}^{3} \mathcal{K}_i$ with $\mathcal{K}_i$ indicates the components containing the sample points coming from the ith vertex of e_h.

b. The recovering point $a = a_0 = (x_0, y_0)$ is the center of the circle, and the sampling points $a_i = (x_i, y_i), i = 1, 2, ..., n(n \ge 4)$ equally distributed around it. we derive

$$|\nabla v(a) - G_h v(a)| \le Ch^2, \quad \forall v \in W_\infty^3(e_h).$$

We use η_t^n and η_{h,e_h} as discretization error indicators in time and space respectively, and then adjust the time step and mesh adaption in the algorithm.

$$\eta_t^n := \|u_h^n - \Pi_n u_h^{n-1}\|, \quad \eta_{h,e_h} := \|G_h u_h - \nabla u_h\|_{0,e_h}, \quad \eta_h^2 = \sum_{e_h \in \mathcal{T}_h} \eta_{h,e_h}^2.$$

During SCR discretization, the time step changes with the error estimate, and the grid size changes according to the time step, so each t_n constructs a new grid, and continues to construct a new space V_h on that grid and Π_n represents the interpolation into the finite element space V_h.

Remark 3.1. *If the gradient is on the boundary $\partial\Omega$, we can treat it in some methods such as a higher order extension, extrapolation, and take the average value.*

Remark 3.2. *The sample points we selected are placed with maximum symmetry around a. On the basis of this, we talk about the sample points in the next two situations. One is that the approximation order can be raised if they are also nodes. The other is that it will only improve recovery accuracy if they are not nodes.*

Remark 3.3. *The SCR strategy can be used not only for the Crank-Nicolson approximation of time-discrete the Cahn-Hilliard equations, but also for other time-discrete formats of the Cahn-Hilliard equations, for example, we can apply to the BDF approximation mentioned in the literature [29] [30], and its stability and unique solvability have been demonstrated. Unlike the format in this paper, the format has three levels of time, so we need u_h^n and u_h^{n-1} to approximate u_h^{n+1}.*

$$\begin{cases} (\dfrac{3u_h^{n+1} - 4\Pi_n u_h^n + \Pi_n u_h^{n-1}}{2\triangle t}, v_h) + (\nabla w_h^{n+1}, \nabla v_h) = 0, & \forall v_h \in V_h, \\ (w_h^{n+1}, \varphi_h) = \varepsilon^2(\nabla u_h^{n+1}, \nabla\varphi_h) + ((u_h^{n+1})^3 - 2\Pi_n u_h^n + \Pi_n u_h^{n-1}, \varphi_h) \\ \qquad\qquad + A\triangle t(\nabla(u_h^{n+1} - \Pi_n u_h^n), \nabla\varphi_h), & \forall \varphi_h \in V_h, \end{cases}$$

4. Numerical experiments

To demonstrate the viability of our strategy, some numerical findings are offered in this section. We discuss a few characteristics of the Cahn-Hilliard Eqs (2.8) and (2.9), which are fully discrete and have various beginning value requirements.

Example 4.1. *In the first test, we use the initial condition listed below to investigate Eq (2.1).*

$$\begin{aligned} u_0(x,y) = \tanh\Big(((x-0.3)^2 + y^2 - 0.2^2)/\varepsilon\Big)\tanh\Big(((x+0.3)^2 + y^2 - 0.2^2)/\varepsilon\Big)\times \\ \tanh\Big((x^2 + (y-0.3)^2 - 0.2^2)/\varepsilon\Big)\tanh\Big((x^2 + (y+0.3)^2 - 0.2^2)/\varepsilon\Big), \end{aligned} \tag{4.1}$$

where the parameter $\Omega = [-1,1]\times[-1,1]$, *and* $\varepsilon = 0.01$.

Sequences of the mesh adaption results and the numerical solutions for six distinct time steps are shown in Figure 1. We can observe that when the node count decreases, the mesh refinement moves in accordance with the level-set zeros. Figure 2 shows the energy level dropping over time. Furthermore, it is also possible to perceive intuitively how the number of nodes and time steps change over time. We see that during the stage of energy's rapid evolution, a small time-step is chosen to capture the change in the numerical solution, and as the system settles into a stable state, the time steps increase.

Example 4.2. *In terms of the Cahn-Hilliard Eq (2.1). Allowing for the following initial condition, let* $\Omega = [-1,1]\times[-1,1]$.

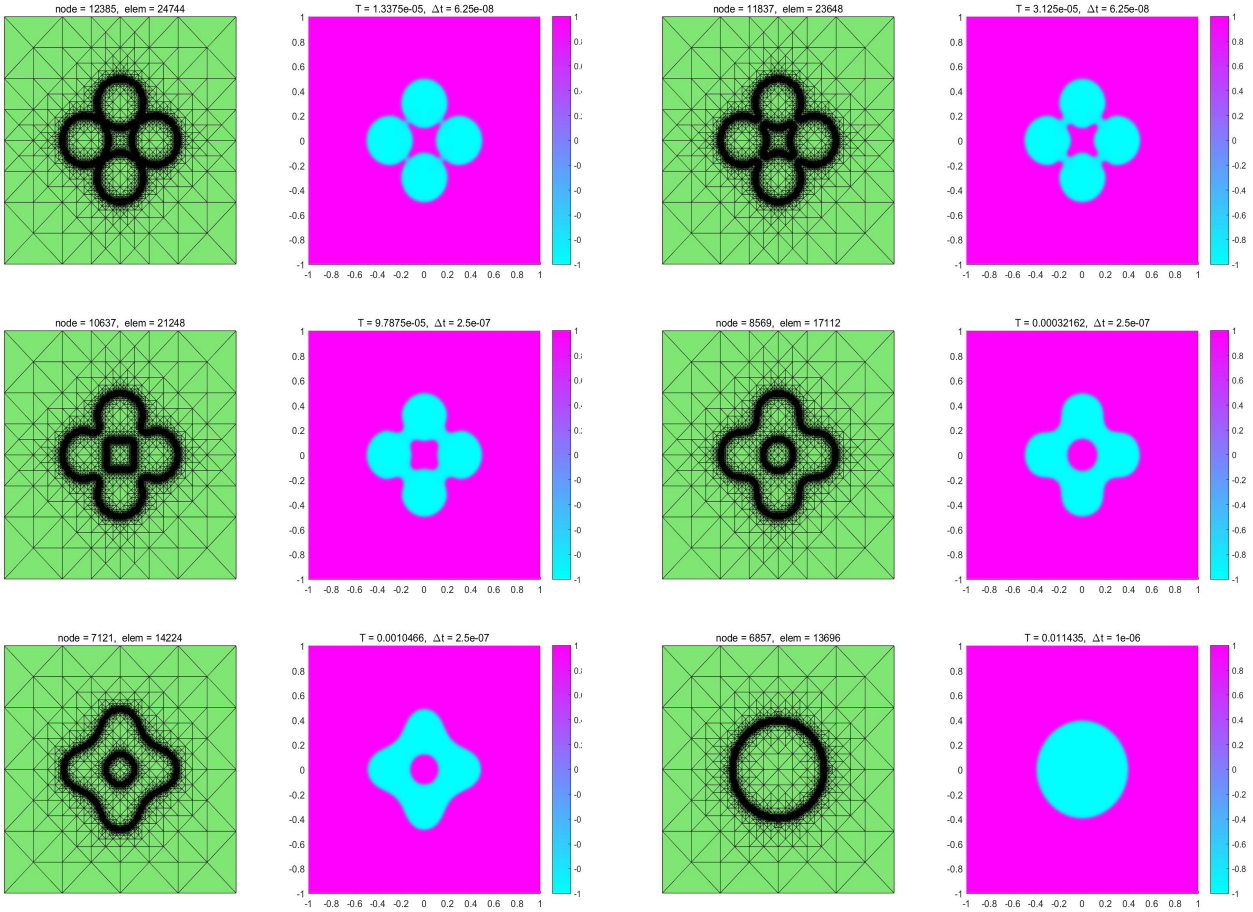

Figure 1. Example 4.1 (CH), results of mesh adaptation and numerical solutions.

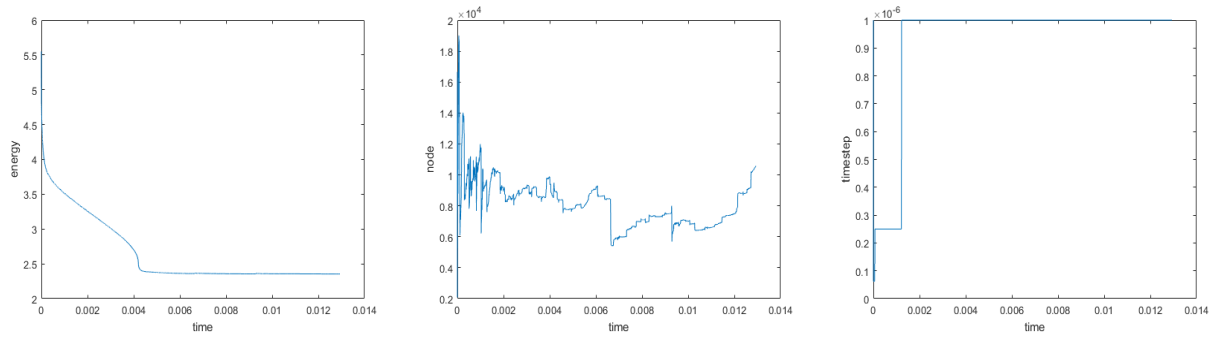

Figure 2. Example 4.1 (CH), from left to right: the distribution of energy, node, and time step.

$$
\begin{aligned}
u_0(x,y) = &\tanh\Big((x^2+y^2-0.15^2)/\varepsilon\Big)\times \\
&\tanh\Big(((x-0.31)^2+y^2-0.15^2)/\varepsilon\Big)\times\tanh\Big(((x+0.31)^2+y^2-0.15^2)/\varepsilon\Big)\times \\
&\tanh\Big((x^2+(y-0.31)^2-0.15^2)/\varepsilon\Big)\times\tanh\Big((x^2+(y+0.31)^2-0.15^2)/\varepsilon\Big)\times \\
&\tanh\Big(((x-0.31)^2+(y-0.31)^2-0.15^2)/\varepsilon\Big)\times \\
&\tanh\Big(((x-0.31)^2+(y+0.31)^2-0.15^2)/\varepsilon\Big)\times \\
&\tanh\Big(((x+0.31)^2+(y-0.31)^2-0.15^2)/\varepsilon\Big)\times \\
&\tanh\Big(((x+0.31)^2+(y+0.31)^2-0.15^2)/\varepsilon\Big),
\end{aligned}
\tag{4.2}
$$

with the parameter $\varepsilon = 0.01$.

In this illustration, Figure 3 shows a succession of mesh adaptation results and their numerical solutions. It is therefore evident via six different time steps that the mesh transformation adapts the rule of the zeros level-set and the number of nodes is decreasing. We infer from Figure 4 that the energy that decays over time, the number of nodes, and the number of time steps all change with time. This numerical result therefore shows that the time steps will grow greater than before when the system stabilizes.

Example 4.3. *In the third example, we apply the following initial value to the Cahn-Hilliard Eq (2.1)*

$$
u_0(x,y) = \tanh\Big(((x-0.3)^2+y^2-0.25^2)/\varepsilon\Big)\tanh\Big(((x+0.3)^2+y^2-0.3^2)/\varepsilon\Big), \tag{4.3}
$$

where the parameter $\Omega = [-1,1]\times[-1,1]$, *and* $\varepsilon = 0.01$.

Figure 5 shows the various adaptive meshes and the associated numerical solutions. It is evident that the mesh transformation applies the level-set rule for zeros. The discrete-time history in Figure 6 also shows that the energy degrades over time. Additionally, Figure 6 shows the connection between time and the quantity of nodes (time-step). In the early stages of the simulation, small steps are used to record changes in the numerical solution, and when the system stabilizes in the latter stages, bigger time steps are used.

Example 4.4. *In the last example, Eq (2.1) with the following initial value was analyzed*

$$
u_0(x,y) = 0.01 rand(x,y), \tag{4.4}
$$

where the parameter $\Omega = [-1,1]\times[-1,1]$, *and* $\varepsilon = 0.01$.

In Figure 7, we plot the different adaptive meshes and their contour plots of the numerical solutions. Figure 8, it displays energy is getting more and more small over time and the distribution of the time steps as well as nodes. We come to the conclusion quite similar to the previous examples.

Remark 4.1. *When* ε *takes a value less than* 0.01, *the change of node number throughout the process still follows the law of zero level set, and the energy is still declining. But the time step will become smaller and the computational cost of the program will become larger, so finally, in the paper we choose* $\varepsilon = 0.01$ *as the experimental result.*

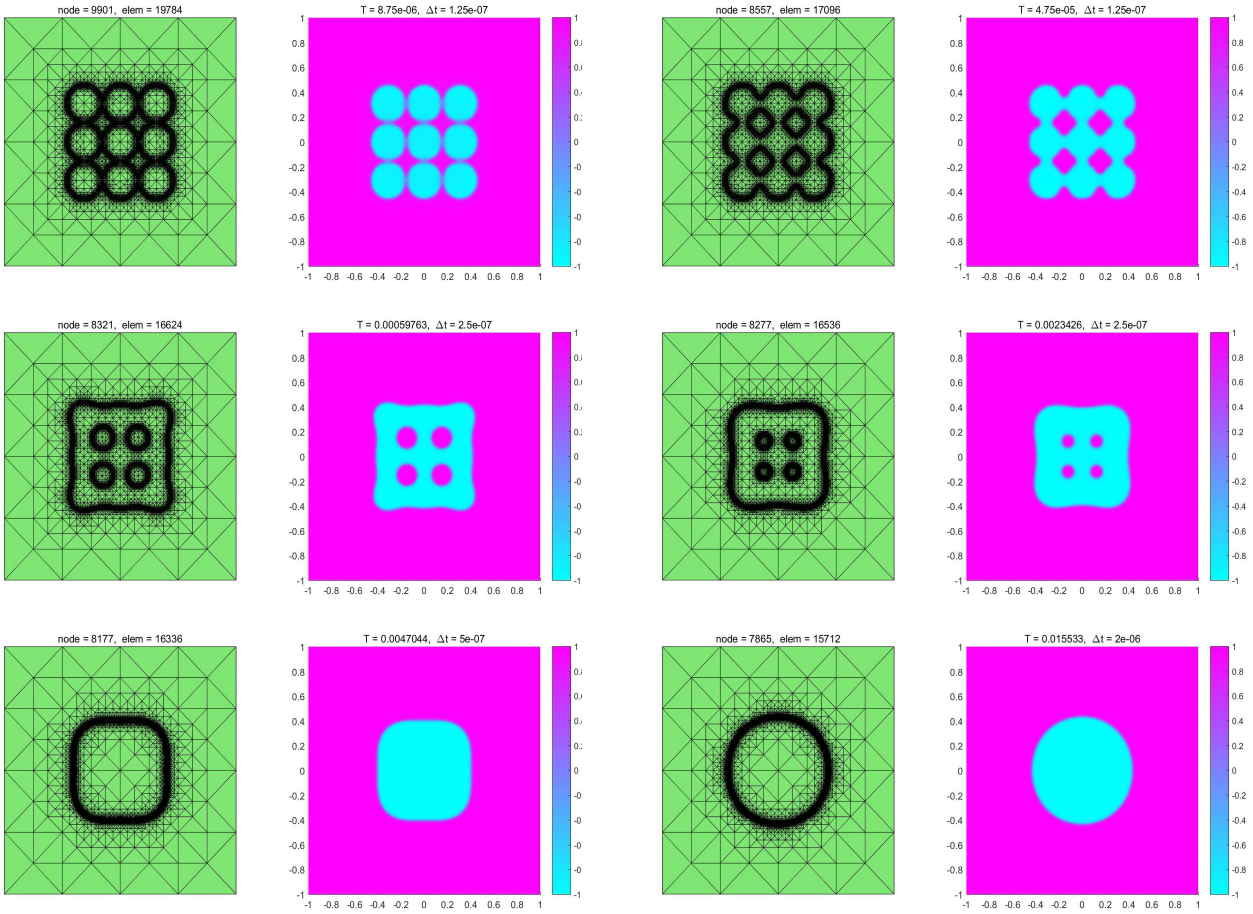

Figure 3. Example 4.2 (CH), results of mesh adaptation and numerical solutions.

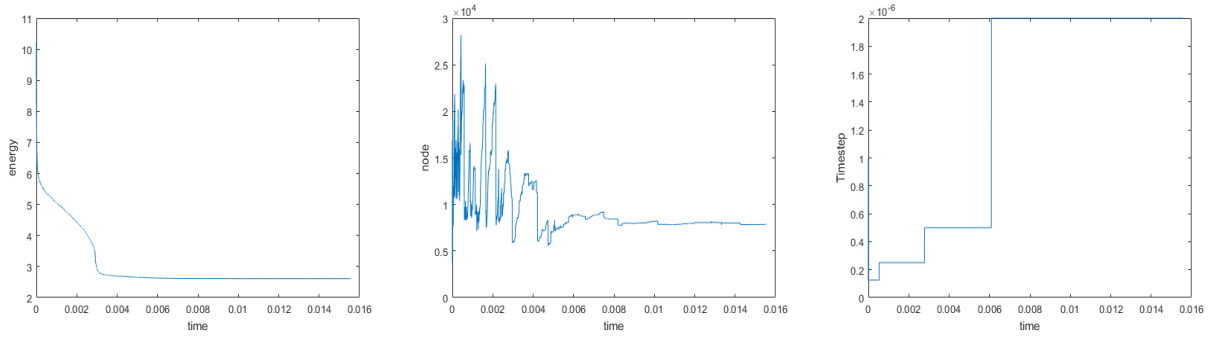

Figure 4. Example 4.2 (CH), from left to right: the distribution of energy, node, and time step.

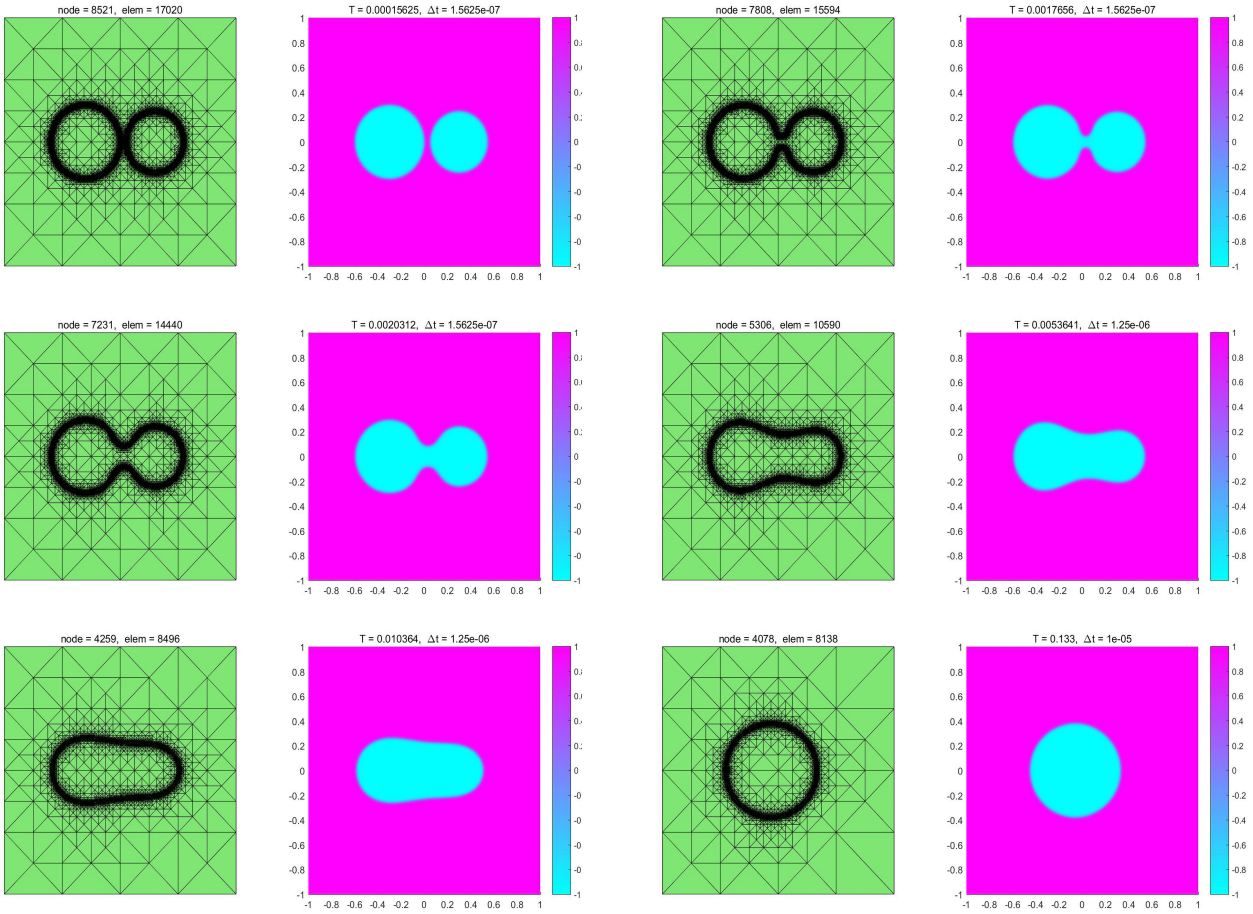

Figure 5. Example 4.3 (CH), results of mesh adaptation and numerical solutions.

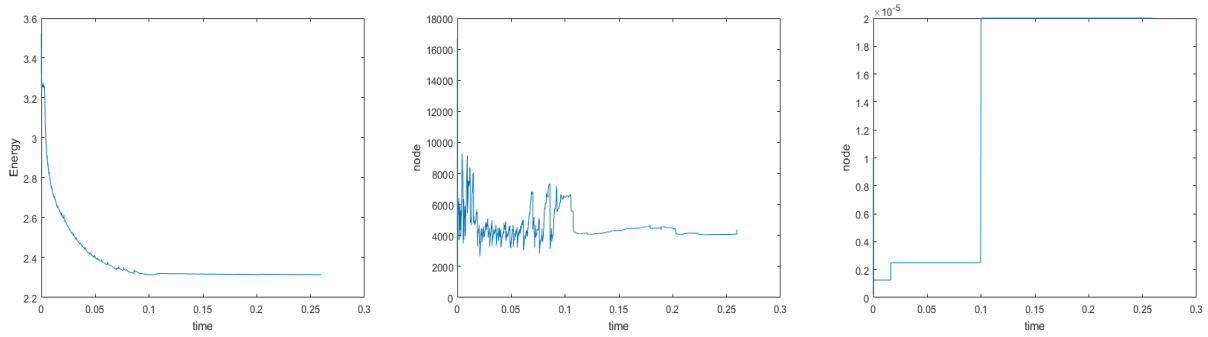

Figure 6. Example 4.3 (CH), from left to right: the distribution of energy, node, and time step.

Table 1 displays the whole discrete format's spatial and temporal precision Eqs (2.8) and (2.9). We take the initial value $u_0(x, y) = 0.01rand(x, y)$, the parameter $\varepsilon = 0.01$, and $T = 1$. Since the precise solution to the initial equation is unknown, the numerical error $e_u^h := u^h(\mathbf{x}, T) - u^{\frac{h}{2}}(\mathbf{x}, T)$ will be determined by the difference between the coarse and fine grids, and the convergence order $log_2(\|e_u^h\|/\|e_u^{\frac{h}{2}}\|)$ will be determined by the ratio of the errors. The table shows that the accuracy converges to 2, which is consistent with our theoretical findings for both spatial and temporal accuracy.

Table 1. The spatial convergence order and the time convergence order when $\varepsilon = 0.01$.

h	$\|u_h^m - u_{\frac{h}{2}}^m\|_0$	*Rate*	$\triangle t$	*Rate*
$\frac{1}{16}$	0.052470400		$\frac{1}{16}$	
$\frac{1}{32}$	0.018185700	1.528700	$\frac{1}{32}$	2.18632
$\frac{1}{64}$	0.003449260	2.398450	$\frac{1}{64}$	2.52708
$\frac{1}{128}$	0.000945365	1.867340	$\frac{1}{128}$	1.78946

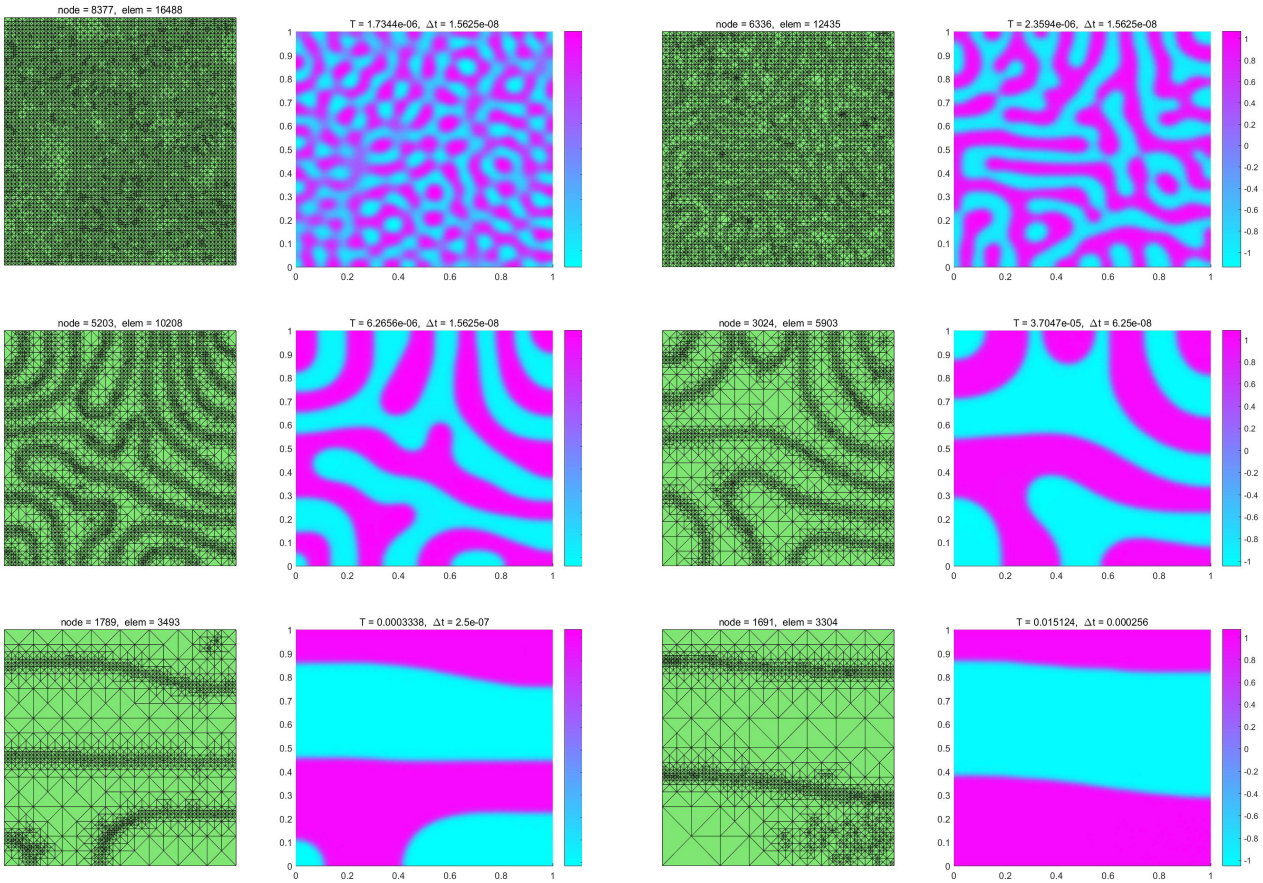

Figure 7. Example 4.4 (CH), results of mesh adaptation and numerical solutions.

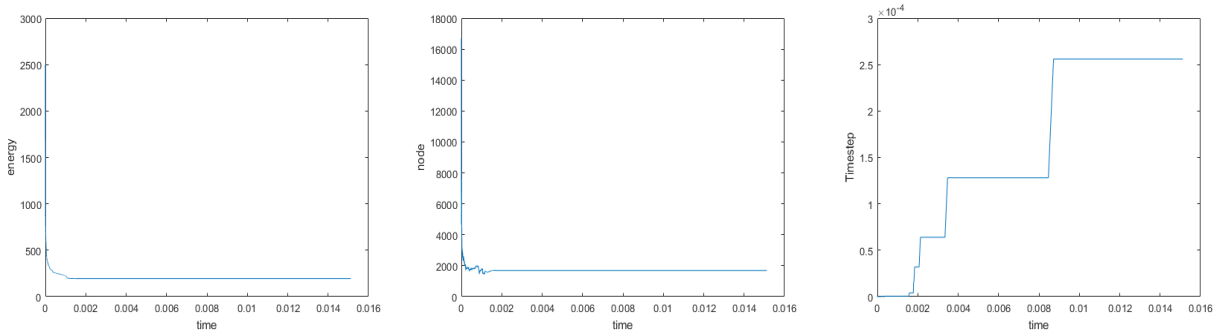

Figure 8. Example 4.4 (CH), from left to right: the distribution of energy, node, and time step.

5. Conclusions

The fundamental idea of this paper is to obtain the spatial discretization operator by SCR method, and then use it as the index of spatial discretization of the Cahn-Hilliard equation. Additionally, the index of temporal discretization is determined by the variation in approximate solutions between adjacent time steps. First of all, in order to solve the Cahn-Hilliard equation, we first develop a second-order scheme that is unconditionally energy stable. Then, the fully discrete system has second-order accuracy both time and space, as determined by error estimation. Finally, these numerical findings are used to demonstrate the efficacy of this approach.

Acknowledgments

Tian's research was supported by Shanxi Scholarship Council of China (No. 2021029) and the 2021 Shanxi Science and Technology Cooperation and Exchange Special Program (No. 202104041101019). Chen's reserach was partially supported by NSFC Project (12201010).

Conflict of interest

No potential conflict of interest was reported by the authors.

References

1. F. Guillen-Gonzalez, G. Tierra, Second order schemes and time-step adaptivity for Allen-Cahn and Cahn-Hilliard models, *Comput. Math. Appl.*, **68** (2014), 821–846. https://doi.org/10.1016/j.camwa.2014.07.014
2. J. Cahn, J. Hilliard, Free energy of a nonuniform system. I. interfacial free energy, *J. Chem. Phys.*, **28** (1958), 258–267. https://doi.org/10.1063/1.1744102
3. A. Karma, W. Rappel, Quantitative phase-field modeling of dendritic growth in two and three dimensions, *Phys. Rev. E*, **57** (1998), 4323–4349. https://doi.org/10.1103/PhysRevE.57.4323

4. S. Allen, J. Cahn, A microscopic theory for antiphase boundary motion and its application to antiphase domain coarsening, *Acta. Matall.*, **27** (1979), 1085–1095. https://doi.org/10.1016/0001-6160(79)90196-2
5. R. Kobayashi, Modeling and numerical simulations of dendritic crystal growth, *Physica D Nonlinear Phenom.*, **63** (1993), 410–423. https://doi.org/10.1016/0167-2789(93)90120-P
6. M. Gurtin, D. Polignone, J. Vinals, Two-phase binary fluids and immiscible fluids described by an order parameter, *Math. Models Methods Appl. Sci.*, **6** (1996), 815–831. https://doi.org/10.1142/S0218202596000341
7. J. Barret, J. Blowey, H. Garcke, Finite element approximation of the Cahn-Hilliard equation with degenerate mobility, *SIAM J. Numer. Anal.*, **37** (1999), 286–318. https://doi.org/10.1137/S0036142997331669
8. C. Elliott, D. French, A nonconforming finite-element method for the two-dimensional Cahn-Hilliard equation, *SIAM J. Numer. Anal.*, **26** (1989), 884–903. https://doi.org/10.1137/0726049
9. C. Elliott, D. French, Numerical studies of the Cahn-Hilliard equation for phase separation, *IMA J. Appl. Math.*, **38** (1987), 97–128. https://doi.org/10.1093/imamat/38.2.97
10. J. Shen, J. Xu, J. Yang, The scalar auxiliary variable (SAV) approach for gradient flows, *J. Comput. Phys.*, **353** (2018), 407–416. https://doi.org/10.1016/j.jcp.2017.10.021
11. S. Zhao, X. Xiao, X. Feng, An efficient time adaptivity based on chemical potential for surface Cahn-Hilliard equation using finite element approximation, *Appl. Math. Comput.*, **369** (2020), 124901. https://doi.org/10.1016/j.amc.2019.124901
12. J. Shen, X. Yang, Numerical approximations of Allen-Cahn and Cahn-Hilliard equations, *Discrete Contin. Dyn. Syst.*, **28** (2010), 1669–1691. https://doi.org/10.3934/dcds.2010.28.1669
13. Y. Huang, W. Yang, H. Wang, J. Cui, Adaptive operator splitting finite element method for Allen-Cahn equation, *Numer. Methods Partial Differ. Equations*, **35** (2019), 1290–1300. https://doi.org/10.1002/num.22350
14. D. Kay, A. Tomasi, Color image segmentation by the Vector-Valued Allen-Cahn Phase-Field Model: A multigrid solution, *IEEE. Trans. Image Process.*, **18** (2009), 2330–2339. https://doi.org/10.1109/TIP.2009.2026678
15. X. Feng, Y. Li, Analysis of interior penalty discontinuous Galerkin methods for the Allen-Cahn equation and the mean curvature flow, *IMA J. Numer. Anal.*, **35** (2015), 1622–1651. https://doi.org/10.1093/imanum/dru058
16. Y. Chen, Y. Huang, N. Yi, A SCR-based error estimation and adaptive finite element method for the Allen-Cahn equation, *Comput. Math. Appl.*, **78** (2019), 204–223. https://doi.org/10.1016/j.camwa.2019.02.022
17. Y. Chen, Y. Huang, N. Yi, A decoupled energy stable adaptive finite element method for Cahn-Hilliard-Navier-Stokes equations, *Commun. Comput. Phys.*, **29** (2021), 1186–1212. https://doi.org/10.4208/cicp.OA-2020-0032
18. D. Mao, L. Shen, A. Zhou, Adaptive finite element algorithms for eigenvalue problems based on local averaging type a posteriori error estimates, *Adv. Comput. Math.*, **25** (2006), 135–160. https://doi.org/10.1007/s10444-004-7617-0

19. Z. Zhang, Z. Qiao, An adaptive time-stepping Strategy for the Cahn-Hilliard Equation, *Commun. Comput. Phys.*, **11** (2012), 1261–1278. https://doi.org/10.4208/cicp.300810.140411s

20. Y. Li, Y. Choi, J. Kim, Computationally efficient adaptive time step method for the Cahn-Hilliard equation, *Comput. Math. Appl.*, **73** (2017), 1855–1864. https://doi.org/10.1016/j.camwa.2017.02.021

21. Y. Huang, N. Yi, The superconvergent cluster recovery method, *J. Sci. Comput.*, **44** (2010), 301–322. https://doi.org/10.1007/s10915-010-9379-9

22. A. Diegel, C. Wang, S. Wise, Stability and convergence of a second order mixed finite element method for the Cahn-Hilliard equation, *arXiv preprint*, 2016, arXiv:1411.5248. https://doi.org/10.48550/arXiv.1411.5248

23. J. Guo, C. Wang, S. Wise, X. Yue, An H^2 convergence of a second-order convex-splitting, finite difference scheme for the three-dimensional Cahn–Hilliard equation, *Commun. Math. Sci.*, **14** (2016), 489–515. https://dx.doi.org/10.4310/CMS.2016.v14.n2.a8

24. K. Cheng, C. Wang, S. Wise, X. Yue, A second-order, weakly energy-stable pseudo-spectral scheme for the Cahn–Hilliard equation and its solution by the homogeneous linear iteration method, *J. Sci. Comput.*, **69** (2016), 1083–1114. https://doi.org/10.1007/s10915-016-0228-3

25. J. Guo, C. Wang, S. Wise, X. Yue, An improved error analysis for a second-order numerical scheme for the Cahn-Hilliard equation, *J. Comput. Appl. Math.*, **388** (2021), 113300. https://doi.org/10.1016/j.cam.2020.113300

26. J. Shen, On error estimates of the projection methods for the Navier-Stokes equations: first-order schemes, *Math. Comput.*, **65** (1996), 1039–1065.

27. X. Feng, A. Prohl, Error analysis of a mixed finite element method for the Cahn-Hilliard equation, *Numer. Math.*, **99** (2004), 47–84. https://doi.org/10.1007/s00211-004-0546-5

28. C. Li, Y. Huang, N. Yi, An unconditionally energy stable second order finite element method for solving the Allen–Cahn equation, *J. Comput. Appl. Math.*, **353** (2019), 38–48. https://doi.org/10.1016/j.cam.2018.12.024

29. Y. Yan, W. Chen, C. Wang, S. Wise, A second-order energy stable BDF numerical scheme for the Cahn-Hilliard equation, *Commun. Comput. Phys.*, **23** (2018), 572–602.

30. K. Cheng, W. Feng, C. Wang, S. Wise, An energy stable fourth order finite difference scheme for the Cahn-Hilliard equation, *J. Comput. Appl. Math.*, **362** (2019), 574–595. https://doi.org/10.1016/j.cam.2018.05.039

AIMS Press